EFFECT OF DIFFERENT PORE SIZES OF POLYURETHANE FOAMS ON PHYSICAL AND MECHANICAL PROPERTIES OF AKERMANITE POROUS SCAFFOLDS

Yanny Marliana Baba Ismail*, Muhammad Syazwan Mohd Noor, Mariatti Jaafar and Ahmad Fauzi Mohd Noor

Biomaterials Niche Group, School of Materials and Mineral Resources Engineering, Engineering Campus, Universiti Sains Malaysia, 14300 Nibong Tebal, Penang.

*yannymarliana@usm.my

Abstract. Various three-dimensional (3D) porous ceramic scaffolds have been introduced as a bone substitute for Tissue Engineering applications, but none is considered ideal for clinical applications. Therefore, this study investigated the effect of using different pore sizes of polyurethane (PU) foam in tailoring the physical and mechanical properties of the novel akermanite porous scaffolds. In this work, the porous scaffolds were prepared using PU foams with 20 and 60 ppi pores sizes, designated as AKr-20 and AKr-60, respectively. These scaffolds were fabricated using as-milled akermanite powders, binder, dispersant, foaming and gelling agents by the combination of gel casting and PU foam replication techniques followed by sintering at 1200°C in air atmosphere. X-ray diffraction (XRD) analysis confirmed that both sintered scaffolds formed pure akermanite phase. Despite different pore sizes used, both scaffolds showed good interconnected pore structure with average pore sizes of 327-722 μm and porosity of 75-82%. AKr-60 scaffolds showed higher compressive strength (2.66 ± 0.83 MPa), which is about 3-fold higher than AKr-20 scaffolds (MPa). At this stage of the study, AKr-60 is selected as a potential substitute material for bone tissue regeneration and repair, particularly for non-load bearing applications.

Keywords: akermanite, porous scaffold, gel-casting, replication technique, pores size

Article Info

Received 11th November 2021
Accepted 15th March 2022
Published 20th April 2022

ISSN: 1823-7010, eISSN: 2600-7444

Introduction

In recent years, bone tissue engineering (BTE) using substitute or intervention material has become an alternative approach in repairing bone defects. Several types of biomaterials such as polymers, metals and ceramics have been explored as future synthetic bone substitute materials [1]. Among these biomaterials, bioceramics have the greatest impact on bone fracture repair due to the chemical and structural similarities relative to the mineral phase of the bone [2]. These bioceramics include calcium phosphate (CaP)-based, bioglass, and silicate-based ceramics.

Akermanite ($Ca_2MgSi_2O_7$) is relatively a new calcium silicate-based bioceramics that have attracted considerable attention due to its good biocompatibility, bioactivity and biodegradability [3-4]. It has been shown that the presence of Ca, Mg and Si in akermanite play important roles in bone formation. Several studies demonstrated that Ca^{2+}, Mg^{2+} and Si^{4+} ions in akermanite structure had a positive influence on cell growth and activities when tested in-vitro and in-vivo [5-6]. It was also reported that the ions released by the dissolution of akermanite through the biodegradation process encourage cell proliferation, osteogenesis (new bone formation) and angiogenesis (blood vessel formation) [7-8]. Additionally, akermanite possesses better mechanical characteristics as compared to CaP-based ceramic such as ß-tricalcium phosphate (ß-TCP), hydroxyapatite (HA) and bioglass [9].

An ideal bone scaffold refers to a porous three-dimensional (3D) scaffold that is specifically designed to closely mimic the composition, architecture, and function of our native bones. Other than composition, architecture and morphological features are also important. These criteria will determine a scaffold's performance to serve as a temporary structure for cell attachment and encourage the formation of bone tissues [10]. The scaffold should have a well-interconnected pores structure with suitable pore sizes (200-500 μm) and an appropriate amount of porosity (40-90%) to enable cell migration, vascularization, and nutrient diffusion [11-12]. It should be mentioned that there is an inverse correlation between pore size and mechanical properties; in general, larger pore sizes reduce the mechanical properties of the scaffolds. To achieve desired characteristics of bone scaffolds, various methods have been employed for the scaffold fabrication, including powder foaming, particle leaching, freeze-drying, gel casting and PU foam replication technique [10, 13]. Among these fabrication techniques, the PU foam replication technique is known to be a simple and economical technique in producing porous bioceramic scaffolds; but this scaffold typically has limited compressive strength as compared to the cortical bone (131-224 MPa) and cancellous bone (5-10 MPa) [14]. On the other hand, gel casting appears to be a better way of fabricating ceramic scaffolds in order to enhance their mechanical strength compared to PU foam replication. However, limitations of this technique lead to non-uniform pore size distribution and less structure of interconnected pores [15]. Therefore, the combination of gel casting and PU replication techniques is proposed in this work as an alternative approach in making novel 3D akermanite porous scaffolds with controllable pore size, porosity, and well-defined interconnected structure. This approach is aimed to improve the mechanical strength of the highly porous brittle bioceramic scaffolds.

Therefore, this study aimed to produce 3D akermanite porous scaffolds using the combination of gel casting and polymeric foam replication techniques and the effect of pore sizes of PU foams on physical properties including phase formation, composition, porosity and architecture (i.e., pores and struts) as well as the mechanical strength of the akermanite scaffolds were investigated. The akermanite porous scaffolds were characterized using X-ray

Diffraction (XRD) analysis, Fourier Transform Infrared (FTIR) spectroscopy, Scanning Electron Microscopy (SEM), porosity measurement and compression test.

Materials and Methods

Preparation of powders. Pure akermanite powders were produced by high-energy high-speed wet planetary ball milling at ambient temperature (27 °C). Calcium oxide, CaO (Sigma-Aldrich, 99.00% pure), magnesium oxide, MgO (Alfa Aesar, 99.00% pure) and silicon dioxide, SiO2 (Sigma-Aldrich, 99.00%) were selected as sources of Ca, Mg and Si, respectively. At first, the raw materials were mixed in deionised water (DI water) with a molar ratio of 2:1:2 according to the basis stoichiometric of akermanite, Ca2MgSi2O7. The mixed powders were then milled for 4 hours in a zirconia jar containing zirconia balls using the planetary ball mill (Retsch PM 100) with the rotational speed of the jar set at 500 rpm. The ball to powder weight ratio was fixed to 10:1 with water to powder ratio of 4:1. The resulting slurry was subsequently dried in the oven at 100°C overnight. Manually ground the dried cake with an agate pestle and mortar and sieved through a 200 μm sieve [16-17].

Fabrication of scaffolds. Commercial polyurethane foam (PU) was used as a sacrificial template to fabricate the novel akermanite porous scaffolds using the combination of gel-casting and polymeric foam replication techniques. Two sets of scaffolds were prepared using different sizes of foams: (1) 20 ppi (AKr-20) and (2) 60 ppi (AKr-60). Firstly, the as-milled akermanite powders were mixed in DI water with a mixture of polyethylene glycol, PEG (Mw= 1500 g/mol, Fluka, Germany) and polyvinyl alcohol, PVA (Mw= 15 000 g/mol, Fluka, Germany) with a ratio fixed at 2:3, dispersant (Dispex A40), sodium dodecyl sulphate, SDS (Sigma-Aldrich) and sorbitol polyglycidyl ether, SPE as foaming and gelling agents, respectively in preparing the ceramic slurry. Then, PU foams were cut into cubes (10 x 10 x 10 mm) and completely immersed in prepared ceramic slurry for 5 minutes. In order to remove the excess slurry and ensure the foams were well impregnated with the ceramic slurry, the coated foams were manually squeezed and released using a pair of glass slides. Afterwards, the coated foams were vacuumed and dried in the oven at 60 °C for 24 hours, before sintering at 1200 °C in an air atmosphere [16-17].

Characterization techniques. The crystalline phase of sintered akermanite porous scaffolds was identified using X-ray diffraction, XRD (Bruker D8). The XRD patterns were recorded in a range of $2\theta = 20^{\circ}$ to 60° with a step size of 0.02 using Cu Kα radiation ($\lambda = 1.541$ Å). The functional groups of sintered scaffolds were also confirmed using Fourier Transform Infrared (FTIR) spectroscopy. Using the KBr pellet technique, the FTIR spectra were scanned in transmittance mode (T%) at wavelength intervals ranging from 400 to 4000 cm^{-1} four times. Morphological observation of the prepared scaffolds was performed using Tabletop Scanning Electron Microscopy (SEM) (TM3000, Hitachi). The average scaffold pore size was determined using SEM micrograph, with 20 measurements were taken for each sample and the sizes of the pore were calculated using Image JTM software (v1.50i.). Archimedes method (ASTM C830-00) was used for the determination of the scaffold porosity, *p* as described by the Equation 1 below.

$$p = \frac{1- (W-D)}{(W-S)} \text{ X } 100 \quad (1)$$

where, W = saturated weight (g), D = dry weight (g) and S = suspended weight (g).

The compression strength of the sintered akermanite scaffolds was carried out using INSTRON 3369 universal tensile machine (ASTM C1424-04) at a crosshead speed of 1.0 mm/min till fractured. The average compressive strength value was obtained from five scaffolds for each set of the prepared scaffold.

Results and Discussion

Physico-chemical analyses. The crystalline phase of the sintered AKr-20 and AKr-60 scaffolds is shown in Figure 1. The XRD patterns confirmed that both prepared scaffolds mainly consist of pure akermanite phase, $Ca_2MgSi_2O_7$ with standard reference pattern code ICDD: 035-0592. This indicated phase stability of akermanite at a high temperature (> 1100 °C). However, the XRD patterns also indicated the existence of diopside, $CaMgSi_2O_6$ (ICDD: 041-1370) as a minor phase. Quantitatively, it can be determined that 95% akermanite and 5% diopside coexist at 1200 °C for both scaffolds, as similarly reported in previous studies [9, 18]. Clearly, the sintered scaffolds have high degrees of crystallinity, as indicated by their sharp and narrow diffraction peaks. Six main peaks of akermanite were detected within the range $20^\circ \leq (2\theta) \leq 60^\circ$, located at about at $2\theta = 23^\circ$, 28 °, 32°, 36°, 44°, and 52° corresponding to (111), (021), (121), (130), (122) and (132), respectively. By using Rietveld refinement analysis, it can be determined that both sintered scaffolds exist in a tetragonal crystal system with a = 7.834 Å and c = 5.008 Å lattice parameters.

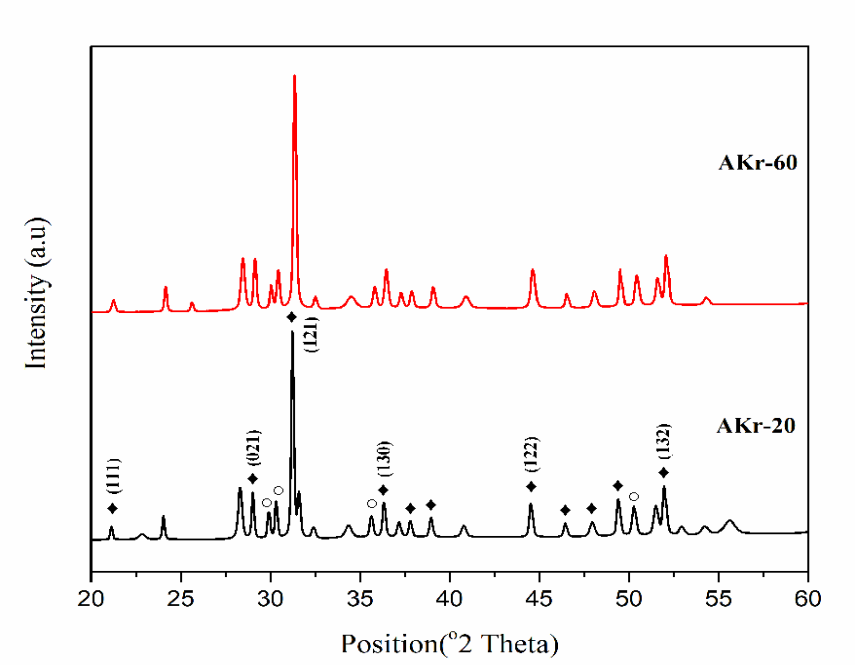

Figure 1. XRD patterns of sintered AKr-60 and AKr-20 scaffolds at 1200 °C, symbols denote (♦) akermanite and (○) diopside.

FTIR spectra (Figure 2) of sintered AKr-20 and AKr-60 scaffolds at 1200 °C were confirmed to present the basic characteristic bands of akermanite structure, which are shown

by O-Ca–O bending modes at 419 cm^{-1} and O–Mg–O bending modes at 487 cm^{-1}. A band at 586 cm^{-1} shows the presence of Ca=O groups and dual bands of O-Si-O were observed at 641 and 683 cm^{-1}. While the sharp bands located at 852, 934 and 973 cm^{-1} were assigned to Si-O stretching modes, as well as the band located at 1021 cm^{-1} presented symmetric stretching mode of Si-O-Si bonds are all consistent with the FTIR patterns of the pure akermanite [16-17]. Finally, the presence of broad moisture adsorption by the hydroxyl (OH^-) groups been detected at 3445 cm^{-1}.

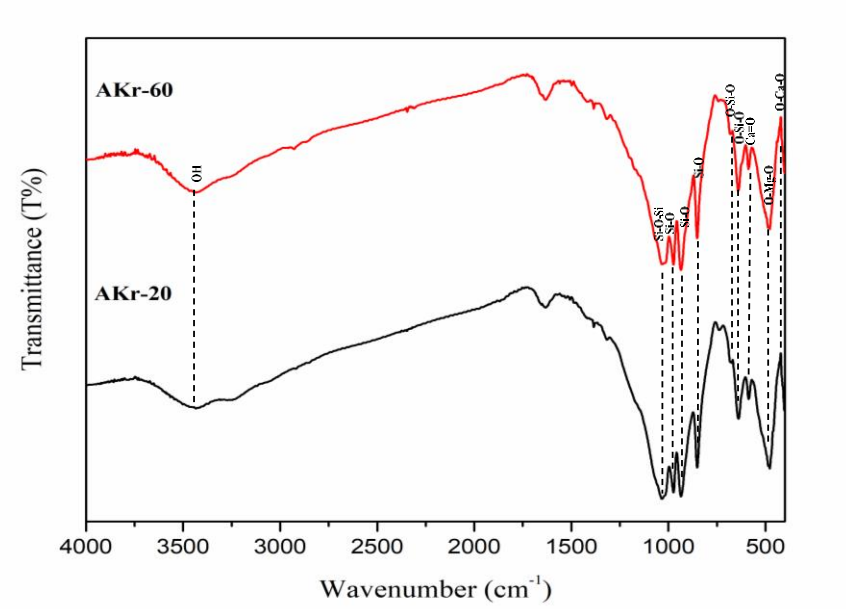

Figure 2. FTIR spectra of sintered AKr-20 and AKr-60 scaffolds at 1200 °C.

Microstructure analysis. Figure 3 shows the internal architecture of sintered AKr-20 and AKr-60 scaffolds prepared using different pore sizes of PU foams. From the morphological observations, these sintered scaffolds showed interconnected pore structures with good bonding formation between the struts. The struts of the sintered scaffolds seem to be fully densified with fewer micro-cracks, indicating the scaffolds were fully sintered at 1200 °C. Scaffolds with good interconnectivity of pores could provide a sufficient supply of nutrients, oxygen, and waste throughout the entire scaffolds via the surrounding vascular network, making it suitable for bone tissue engineering applications. [19]. The average pore sizes of AKr-60 scaffolds (327 ± 55.00 µm) obtained was also found to fall in a range of ideal pore size for bone scaffolds [20]. However, AKr-20 scaffolds possess a relatively larger pore size distribution (721.60 ± 87.80 µm) than AKr-60.

Samples	Internal architecture	Average pore size (µm)
AKr-20	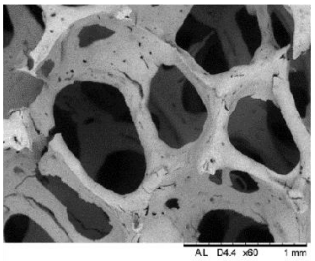	721.60 ± 87.80
AKr-60	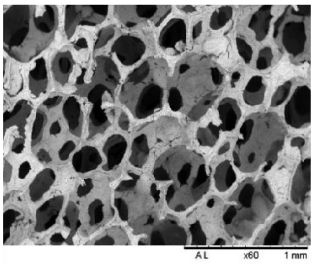	327.00 ± 55.00

Figure 3. Comparison of the internal architecture sintered AKr-20 and AKr-60 scaffolds prepared. Scale bar = 1 mm.

Mechanical properties. A comparison of the compressive strength of sintered scaffolds with different pore sizes of PU foams is shown in Table 1. As expected, the decrease in the compressive strength is a result of the larger interconnected pore size of the scaffold. In fact, increasing the pore size tends to higher pore surface area, therefore this in turn could affect the mechanical strength of the scaffold. Clearly, AKr-60 scaffolds showed a significantly higher compressive strength of 2.66 ± 0.83 MPa, which was about 3-folds of that for AKr-20 scaffolds (0.65 ± 0.20 MPa). This trend is consistent with the SEM observation, showing that the internal architecture of sintered scaffolds may affect mechanical properties substantially. In addition, both sintered scaffolds prepared using this technique could be controlled to have a porosity ranging between 75-82%, which is favourable for the biological environment [21].

Table 1. Total porosity and compressive strength of sintered scaffolds subjected to different size pores of PU foams.

Samples	Total porosity (%)	Compressive strength (MPa)
AKr-20	75.90	0.65 ± 0.20
AKr-60	81.83	2.66 ± 0.83

Conclusion

3D akermanite porous scaffolds with different pore sizes of foams had been prepared via a combination of gel-casting and PU foam replication techniques. Both of the fabricated scaffolds (AKr-20 and AKr-60) consist of akermanite as the major phase at 1200 °C. Akermanite ceramics prepared by this new technique produced scaffolds with desired architecture features and possess interconnected pore structures with suitable pore size distribution. In terms of mechanical strength, smaller pore size showed significantly higher mechanical strength with AKr-60 scaffolds (60 ppi) having about 3-folds higher compressive strength than AKr-20 scaffolds (20 ppi). At this point, it can be concluded that AKr-60 shows the optimum properties as a potential material for the bone substitute, particularly in non-load bearing applications.

Acknowledgements

The financial support for this research was provided by the Ministry of Higher Education Malaysia under Fundamental Research Grant Scheme (FRGS) Grant no. FRGS/1/2021/ TK0/USM/03/4.

Author Contributions

All authors contributed toward data analysis, drafting and critically revising the paper and agree to be accountable for all aspects of the work.

Disclosure of Conflict of Interest

The authors have no disclosures to declare

Compliance with Ethical Standards

The work is compliant with ethical standards

References

[1] Bose, S. & Sarkar, N. (2020). Natural Medicinal Compounds in Bone Tissue Engineering. *Trends Biotechnol*., 38 (4) 404–417.

[2] Pasandideh, Z., Tajabadi, M., Javadpour, J. & Mirkazemi, S. M. (2020). The effects of Fe3+ and Co^{2+}substitution in $Ca_{10-x-y}\ Fe_xCo_y\ (PO_4)_6(OH)_2$ hydroxyapatite nanoparticles: magnetic, antibacterial, and improved drug release behavior. *Ceram. Int.*, 46(10) 16104–16118.

[3] Han, Z., Feng, P., Gao, C., Shen, Y., Shuai, C. & Peng, S. (2014). Microstructure, mechanical properties and in vitro bioactivity of akermanite scaffolds fabricated by laser sintering. *Biomed. Mater. Eng.*, 24(6) 2073–2080.

[4] Liu, A., Sun, M., Yang, X., Ma, C., Liu, Y., Yang, X. & Gou, Z. (2016). Three-dimensional printing akermanite porous scaffolds for load-bearing bone defect repair: An investigation of osteogenic capability and mechanical evolution. *J. Biomater. Appl.,* 31(5) 650–660.

[5] Tavangarian, F., Zolko, C. A., Sadeghzade, S., Fayed, M. & Davami K. (2020). Fabrication, Mechanical Properties and In-Vitro Behavior of Akermanite Bioceramic. *Materials.,* 13(21) 1–13.

[6] Arastouei, M., Khodaei, M., Atyabi, S. M. & Nodoushan, M. J. (2020). Poly lactic acid-akermanite composite scaffolds prepared by fused filament fabrication for bone tissue engineering. *J. Mater. Res. Technol.,* 9(6) 14540–14548.

[7] Tavangarian, F., Zolko, C. A. & Davami, K. (2021). Synthesis, characterization and formation mechanisms of nanocrystalline akermanite powder. *J. Mater. Res. Technol.,* (11) 792–800.

[8] Bafandeh, M. R., Mojarrabian, H. M. & Doostmohammadi, A. (2019). Poly (vinyl alcohol)/chitosan/akermanite nanofibrous scaffolds prepared by electrospinning. *J. Macromol. Sci. Part B Phys.,* 58(9) 749–759.

[9] Myat-Htun, M., Mohammadi, H., Ahmad-Fauzi, M.N., Kawashita, M. & Yanny Marliana, B.I. (2021). Comprehensive investigation of phase formation mechanism and physico-mechanical properties of Ca-Mg-silicate. *ASEAN Eng., J.* 11(2) 37–50.

[10] Saba G., Hesaraki S. & Hajisafari M. (2018). Utilization of rheological parameters for the prediction of β-TCP suspension suitability to fabricate bone tissue engineering scaffold through foam replication method. *J. Aust. Ceram. Soc.,* 54(4) 587–599.

[11] Karamian, E., Nasehi, A., Saber-Samandari,, S. & Khandan, A. (2017). Fabrication of hydroxyapatite-baghdadite nanocomposite scaffolds coated by PCL/Bioglass with polyurethane polymeric sponge technique. *Nano. J.,* 4(3) 177-183.

[12] Muhammad Syazwan, M.N., Ahmad-Fauzi,, M. N., Balestri, W. Reinwald, Y., & Yanny Marliana, B.I. (2021). Influence of ternary divalent cations (Mg2+, Co2+, Sr2+) substitution on the physicochemical, mechanical and biological properties of carbonated hydroxyapatite scaffolds. *J. Aust. Ceram. Soc.,* 57 1499–1510.

[13] Roseti, L., Parisi,V., Petretta, M., Cavallo, C., Desando, G., Bartolotti, I. & Grigolo, B. (2017). Scaffolds for bone tissue engineering: state of the art and new perspectives. *Mater. Sci. Eng. C,* 78 1246–1262.

[14] Sheikh, Z., Najeeb, S., Khurshid, Z., Verma, V., Rashid, H. & Glogauer, M. (2015). Review: Biodegradable Materials for Bone Repair and Tissue Engineering Applications. *Materials,* 8 5744-5794.

[15] Dash, S. R., Sarkar, R. & Bhattacharyya, S. (2015). Gel casting of hydroxyapatite with naphthalene as pore former. *Ceram. Int.,* 41(3) 3775–3790.

[16] Myat-Htun,, M., Mohammadi, H., Ahmad-Fauzi, M.N., Kawashita, M. & Yanny Marliana, B.I. (2020). Enhanced sinterability and in vitro bioactivity of barium-doped akermanite ceramic. *Ceram. Int.,* 46(11) 19062–19068.

[17] Mohammadi, H., Myat-Htun, M., Yanny Marliana, B.I., Shariff, K. A. & Ahmad-Fauzi, M.N. (2019). Structural, physicomechanical, and in vitro biodegradation studies on Sr-doped bioactive ceramic. *Ceram. Int.,* 45(11) 14090–14097.

[18] Choudhary, R., Koppala,, S. & Swamiappan S. (2015). Bioactivity studies of calcium magnesium silicate prepared from eggshell waste by sol–gel combustion synthesis. *J. Asian Ceram. Soc.,* 3(2) 173–177.

[19] Chocholata, P., Kulda V. & Babuska V. (2019). Fabrication of scaffolds for bone-tissue regeneration. *Materials,* 12(4) 568.

[20] Muhammad, Syazwan M.N., Ahmad-Fauzi M. N., Balestri, W., Reinwald, Y. & Yanny Marliana B.I. (2021). Effectiveness of various sintering aids on the densification and in vitro properties, of carbonated hydroxyapatite porous scaffolds produced by foam replication technique. *Mater. Today Commun.,* 27 102395.

[21] Min, S. H., Jin, H. H., Park, H. Y., Park, I. M., Park,, H. C. & Yoo,n S. Y. (2006). Preparation of porous hydroxyapatite scaffolds for bone tissue engineering. *Mater. Sci. Forum,* 510 754–757.